Preprints (www.preprints.org) | NOT PEER-REVIEWED | Posted: 24 May 2018 doi:10.20944/preprints201805.0336.v1

Peer-reviewed version available at *Materials* **2018**, *11*, 1555; doi:10.3390/ma11091555

Article

In vitro osteogenesis stimulation via nano-hydroxyapatite/carbon nanotube thin films on biomedical stainless steel

Natalia M. Martinelli [1], Maria Julia G. Ribeiro [1], Ritchelli Ricci [1], Miller A. Marques [1], Anderson Oliveira Lobo [1,2,3] and Fernanda Roberta Marciano [1,2,*]

[1] Instituto de Pesquisa e Desenvolvimento, Universidade do Vale do Paraíba, Av. Shishima Hifumi, nº 2911, Bairro Urbanova, São José dos Campos, São Paulo, CEP: 12244-000, Brazil
[2] Instituto de Ciência e Tecnologia, Universidade Brasil, Rua Carolina da Fonseca, 584, Bairro Itaquera, São Paulo, CEP: 08230-030, Brazil
[3] Laboratório Interdisciplinar de Materiais Avançados, Programa de Pós-Graduação em Ciência e Engenharia dos Materiais, Universidade Federal do Piauí, Campus Universitário Ministro Petrônio Portella, Bairro Ininga, Teresina, Piauí, CEP: 64049-550, Brazil
* Correspondence: frmarciano@pq.cnpq.br and femarciano@gmail.com

Abstract: Herein, we evaluated the electrophoretic deposition of nanohydroxyapatite/superhydrophilic multiwalled carbon nanotube composites (nHAp/MWCNT) onto stainless steel biomedical alloys for applications in bone tissue engineering. First, nHAp/MWCNT composites were dispersed into 0.042 mol L^{-1} of $Ca(NO_3)_2.4H_2O$ + 0.025 mol L^{-1} $NH_4H_2PO_4$ electrolytes (pH=4.8) at two different concentrations. Next, a voltage of -2V was applied using 316L stainless steel as a working electrode and (0.27 cm^2), a high-purity platinum coil wire as the auxiliary electrode, and an Ag/AgCl(3 M) electrode was used as the reference electrode. The nHAp/MWCNT composites were characterized by transmission electron microscopy. The deposited nHAp and nHAp/MWCNT films were characterized by profilometry, scanning electron microscopy, X-Ray diffractometry and Raman spectroscopy. Human osteoblast cells were cultivated with the different materials, and *in vitro* cytotoxicity was evaluated using lactate dehydrogenase (LDH) assay. The osteogenesis process was evaluated by mRNA levels of the three genes that are directly related to bone repair: Alkaline Phosphatase, Osteopontin and Osteocalcin. We showed that rough, crystalline apatite thin films containing phases of nHAp were successfully deposited onto 316L stainless steel alloys. Also, we noticed that nHAp/MWCNT thin films deposited onto 316L stainless steel alloys upregulated the expression of important genes related to bone mineralization and maturation. Our results strongly support the possibility of this new alternative to modify the surface of metallic biomedical alloys to promote bone tissue regeneration.

Keywords: 316L; electrodeposition; nano-hydroxyapatite; carbon nanotubes; osteoblasts; gene expression

1. Introduction

Metallic alloys are the most common metal used to fabricate protheses that promote bone tissue regeneration during the last few decades. Different metal alloys have been used as implants, such as 316L stainless steel [1], Ti6Al4V [2], cobalt alloy [3], titanium, Niquel-Titanium, among others [4]. These have many advantages, including high corrosion resistance, desirable mechanical properties, and partial biocompatibility. Moreover, 316L stainless steel specifically has a lower cost than others, and thus can be an alternative to more people, especially in emergent countries [5,6]; however, none

© 2018 by the author(s). Distributed under a Creative Commons CC BY license.

Preprints (www.preprints.org) | NOT PEER-REVIEWED | Posted: 24 May 2018 doi:10.20944/preprints201805.0336.v1

Peer-reviewed version available at Materials 2018, 11, 1555; doi:10.3390/ma11091555

of these materials have not been applied to long-term clinical application, especially because they can corrode in biological environments, thereby causing implant failure. To solve problems related to corrosion, chemical modification and deposition of thin micro- and nano-films have been proposed as a solution to this challenge [6,7].

Nanofeature structures are promising because they are similar to the natural components of the extracellular matrix, making them extremely important in the field of bioengineering. Their configurations and physicochemical properties influence the cellular interactions, leading to tissue regeneration, and thus have incredible potential for the development of improved implantable surfaces [8].

Calcium phosphates associated to carbon materials have been widely used in experimental *in vitro* and *in vivo* assays to evaluate their potential for use as bone substitutes, due to their excellent biocompatibility, guided bone regeneration, and osteoconductive properties. We recently patented a novel class of nanobiomaterials based on a pioneering method of ultrasound-assisted deposition of nHAp onto superhydrophilic multiwalled carbon nanotube (MWCNT) scaffolds [9]. Furthermore, in a very recent *in vitro* study, we systematically evaluated the production and characterization of these nanocomposites, focusing on their physical, chemical and biological properties [10]. We showed that nHAp/MWCNT nanocomposites were bioactive and suitable for biomedical applications, with a demonstrated bactericidal effect against *Staphylococcus aureus* (*S. aureus*) and *Escherichia coli* (*E. coli*), with no osteoblast cytotoxicity.

Different techniques have been applied to obtain nHAp thin films with and without the association of carbon nanotubes (CNT) onto biomedical metal alloys. Many alternatives have been applied to obtain thin and homogeneous films onto metallic implants: a shear mixing method [17, 18], sprayed plasma [19–20], electrophoretic deposition [11, 21] and electrodeposition [2, 14]. Among them, electrodeposition is a simple technique to synthesize HAp/CNT coatings. This method is conducted at low temperature, allows for good control over the deposition thickness and quality, consumes a low amount of energy, and is an environmental friendly process.

Herein, a cost-effective and versatile coating technique was applied to obtain nanofeatures onto 316L stainless steel alloys using electrodeposition. A thin and homogeneous high crystalline nHAp/MWCNT composite thin films were electrodeposited onto 316L stainless steel alloys and their chemical, structural and surface properties were evaluated. The *in vitro* osteogenesis process was also evaluated using human osteoblast cells up to 14 days. The developed nHAp/MWCNT thin films showed superior biological properties, enhancing genes related to mineralization and maturation of human osteoblast cells.

2. Materials and methods

2.1. Electrophoretic deposition

10 × 10 × 1 mm 316L stainless steel samples were polished, cleaned in acetone using ultrasound, and dried under ambient room temperature. nHAp/MWCNT composite and hydroxyapatite were produced as previously reported [11] and characterized by high resolution transmission electron microscopy (FEI-Tecnai G_2 F20). 0.042 mol L^{-1} of $Ca(NO_3)_2.4H_2O$ + 0.025 mol L^{-1} $NH_4H_2PO_4$ electrolytes (pH=4.8) were heated at 70°C. Then, 10 mg/mL of two different concentrations of nHAp/MWCNT (1 and 2% of CNT into nHAp matrix) and 10 mg/mL of nHAp (1%) were dispersed using an ultrasound (Sonic Vibra-Cell VCX 500) for 30 minutes. The electrophoretic process was carried out using a classical electrophoretic apparatus (Autolab, PGSTAT 128N, Netherland). 316L stainless steel alloys were used as working electrodes (0.27 cm^2), a high-purity platinum coil wire used as the auxiliary electrode, and an Ag/AgCl (3 M) electrode used as the reference electrode. The electrochemical parameters were as follows: applied voltage at -5V and for 7200 seconds.

2.2. Characterization of nHAp/MWCNT thin films

The nHAp crystalline phases were identified using an X-ray diffraction instrument (X-Pert Philips) with Cu Kα radiation (λ = 0.154056 nm) with a 2θ angle of 10° to 50° under the following

Preprints (www.preprints.org) | NOT PEER-REVIEWED | Posted: 24 May 2018 doi:10.20944/preprints201805.0336.v1

Peer-reviewed version available at Materials 2018, 11, 1555; doi:10.3390/ma11091555

conditions: voltage of 40 kV, current of 30 mA, step size of 0.02°, and counting time of 2 s per step. The electrodeposited thin film morphology and roughness value were characterized by an optical 3D profilometry (Wyko, Modelo NT 1100, Veeco, EUA). The diffraction peaks were indexed according to the Joint Committee on Powder Diffraction Standards (JCPDS). The crystal sizes were calculated using Scherrer equation ($D_{hkl}=k\lambda/\beta_{\cos(\theta)}$). The structural analyses of deposited nHAp/MWCNT thin films was identified using Raman spectroscopy (Renishaw, model 2000). The spectra were collected after 30 seconds. The data were plotted using Origin Lab 8®.

2.3. Cytotoxicity test

MG-63 (ATCC® CRL-1427™) human osteoblast cell line was used in this study. The culture medium was Dulbecco's Modified Eagle Medium (DMEM) supplemented with 10% fetal bovine serum (FBS), 100 IU mL^{-1} of penicillin and 100 μg mL^{-1} of streptomycin. Cells were cultured at 37ºC in a 5%CO_2 humidified incubator. To assess cell viability, we used the LDH assay (TOX7-1KT Sigma). The procedures were done in accordance with manufacturer protocol. The following groups were used: 316L stainless steel, 316L stainless steel covered with (a) nHAp (named nHAp), (b) nHAp/MWCNT_1% (named nHAp/MWCNT_1%), or (c) nHAp/MWCNT_3% (named nHAp/MWCNT_3%), cells (positive control), and DMSO (negative control). Prior to the biological tests, all the samples were sterilized for 24 h under UV irradiation and placed in individual wells of 24-well culture plates. The cells were seeded in each well at a concentration of 2 × 10^5 cells/mL, supplemented with 10% FBS, with CO_2 (5%) at 37 °C. After 24 h, 50 μL (1/10 vol.) lysis solution was added and plated for 45 min. Next, 100 μL of LDH were added at each well. After this stage, 150 μL was transferred to a 96-well plate and incubated at room temperature for 30 minutes (dark). To finalize the reaction, 50 μL of 1M HCl were added to each well. The optical densities (ODs) were measured at a wavelength of 490 nm and 690 nm (Spectra Count, Packard).

The results were analyzed using GraphPad Prism InStat software (version 6.1 San Diego, CA, USA), the ANOVA test (one-way) was used, followed by the Kruskal-Wallis test, considering statistically significant the samples with $p<0.01$ (n=3).

2.4. Gene expression analysis

Three genes involved in bone repair were evaluated by RT-qPCR amplifications. *ALPL* (alkaline phosphatase), *OPN* (osteopontin) and *OC* (osteocalcin) were performed in triplicate on an ABI Prism 7500 Sequence Detection System (Applied Biosystems, Foster City, CA, USA) using kit GoTaq® qPCR Master Mix (Promega, São Paulo, Brasil).

RNA extraction was performed using Trizol® Reagent (Life Technologies, Rockville, MD, USA). RNA integrity was assessed using 1.5% agarose gel electrophoresis to analyze the 18S and 28S bands. Results were quantified by ultraviolet absorption spectroscopy using NanoDrop equipment (280/260 and 260/230, ND-1000 Spectrophotometer v.3.0.7 - Labtrade). cDNA synthesis reactions were carried out using a thermal cycler (Biocycler, MJ96G, USA) and 2 g of RNA through a reverse transcription reaction following the manufacturer's instructions of the commercial kit (ImProm-II™ Reverse Transcription System, Promega, São Paulo, Brazil). Reverse transcription (RT) was carried out for 5 min at 25ºC, then 60 min at 42ºC, and finally followed by 15 min at 70º C, and the reaction mixture was stored at -20ºC.

The primers for amplification of five target genes and reference genes were determined using IDT software (Integrated DNA Technologies/ available on: http://www.idtdna.com) and Primer-Blast software (available on: http://www.ncbi.nlm.nih.gov/tools/primer-blast). All primers used are listed in Table 1. Data were normalized based on the expression of the reference gene. We quantified the transcripts of housekeeping genes *GAPDH* (glyceraldehyde 3-phosphate dehydrogenase), *18SrRNA* (18S ribosomal RNA), and *β-actin* (Actin smooth muscle-beta) and selected as endogenous control *β-actin* gene, which provided increased accuracy and resolution in the quantification of gene expression data, facilitating the detection of smaller changes in gene expression than otherwise possible. Standard PCR conditions were used: 5 min at 95 °C, 40 cycles of 15 seconds at 95°C, 1 min at 60 °C, and finally 5 min at 72 °C.

Preprints (www.preprints.org) | NOT PEER-REVIEWED | Posted: 24 May 2018 doi:10.20944/preprints201805.0336.v1

Peer-reviewed version available at Materials 2018, 11, 1555; doi:10.3390/ma11091555

143 **Table 1.** Details of gene-specific used in RT- qPCR assay.

Gene symbol/ (access number)	*Gene name*	*Primer sequences*	*Function*
β-actin / *ACTB* (NM_001101)	Actin Beta	5′-ACCAACTGGGACGACATGGAGAAA-3′ 5′-TAGCACAGCCTGGATAGCAACGTA-3	Highly conserved protein that are involved in cell motility, structure, and integrity
ALPL (NM_000478.4)	Alkaline phosphatase	5′-CCGTGGCAACTCTATCTTTGG-3 5′-GCCATACAGGATGGCAGTGA-3	This enzyme may play a role in bone mineralization
OPN / *SPP1* (NM_1251830)	Secreted phosphoprotein 1/ Osteopontin	5′-AGACACATATGATGGCCGAG-3 5′-GGCCTTGTATGCACCATTCAA-3	Protein involved in the attachment of osteoclasts to the mineralized bone matrix. Secreted and binds hydroxyapatite with high affinity
OC / *BGLAP (NM_199173)*	Osteocalcin/ Bone gamma-carboxyglutamate protein/	5′-AAGAGACCCAGGCGCTACCT-3 5′-AACTCGTCACAGTCCCGGATTG-3	Highly abundant bone protein secreted by osteoblasts that regulates bone remodeling

144 Measurements of gene expression were calculated using the relative Delta-Delta Ct (ΔΔCt)
145 method, in which the average value of Cts (cycle threshold) were obtained for the target genes and
146 compared with the average of the Cts endogenous gene [12]. These values were normalized by the
147 average of the control samples, and the resulting values of fold-change thus relative to the control
148 (Relative Quantification, RQ).
149 The results of the RT-qPCR were analyzed using the ANOVA (one-way) test, followed by
150 Dunnett's multiple-post test, considering statistically significant samples with $p<0.05$, both in the
151 GraphPad Prism program version 6.1.

152 **3. Results**

153 The characterization of nHAp/MWCNT before and after electrophoretic process is summarized
154 in **Fig. 1**. The internal structures of MWCNTs are shown in **Fig. 1a.** The tubes have outer diameters
155 around 60 nm and internal wall diameters around 50 nm. The MWCNTs did not have any impurities
156 and had a typical internal bamboo-like structure. The purity is related to the synthesis method and
157 the acid and thermal treatment applied prior to the nanocomposite fabrication [13]. Two different
158 regions were noticed upon analysis of nHAp/MWCNT composites: (a) MWCNT completely covered
159 by nHAp crystals (15 nm in diameter; square region, **Fig. 1b**) and (b) nHAp agglomerates (circle
160 region, **Fig. 1b**). We postulate that the production of nHAp/MWCNT composites is partially
161 homogeneous.

Preprints (www.preprints.org) | NOT PEER-REVIEWED | Posted: 24 May 2018 doi:10.20944/preprints201805.0336.v1

Peer-reviewed version available at Materials 2018, 11, 1555; doi:10.3390/ma11091555

The ultrasound process is a good way to produce nano-ceramic composites, and highly crystalline structures can be produced, especially calcium phosphate structures [14]. Raman spectra collected from all the analyzed samples (**Fig. 1c**) show typical bands attributed to nHAp. Also, we observed the first D and G (1330-1590 cm^{-1}) order band from CNTs [15]. The peak at 961 cm^{-1}, sharp peak at 1030–1050 cm^{-1}, and lower intensity peaks at ~ 420, 580, and 780 cm^{-1} are typically attributed to crystalline apatite structures, more evident in nHAp phase [16,17]. **Fig. 1d** shows the X-ray diffraction pattern of the nHAp/MWCNT deposited onto 3l6L stainless steel at two different concentrations. The main peaks attributed to hydroxyapatite were indexed with the JCPDS:024-0033 card (asterisk). The 002 plane [18] was used to calculate the crystal size using the Scherrer equation ($r = 0.89\lambda/B\cos\theta$). Each nHAp crystal orientation is specified in the XRD pattern, where the main diffraction peaks of HA appear around 28°. The crystal size changed in accordance to nHAp/MWCNT concentration. When 1% of nHAp/MWCNT composite was used, crystal size was 61.3 nm. In contrast, when 3% was used, a 24.5 nm crystal size was calculated. This result should be noted, and can be correlated directly to surface roughness measured from the electrodeposited thin films.

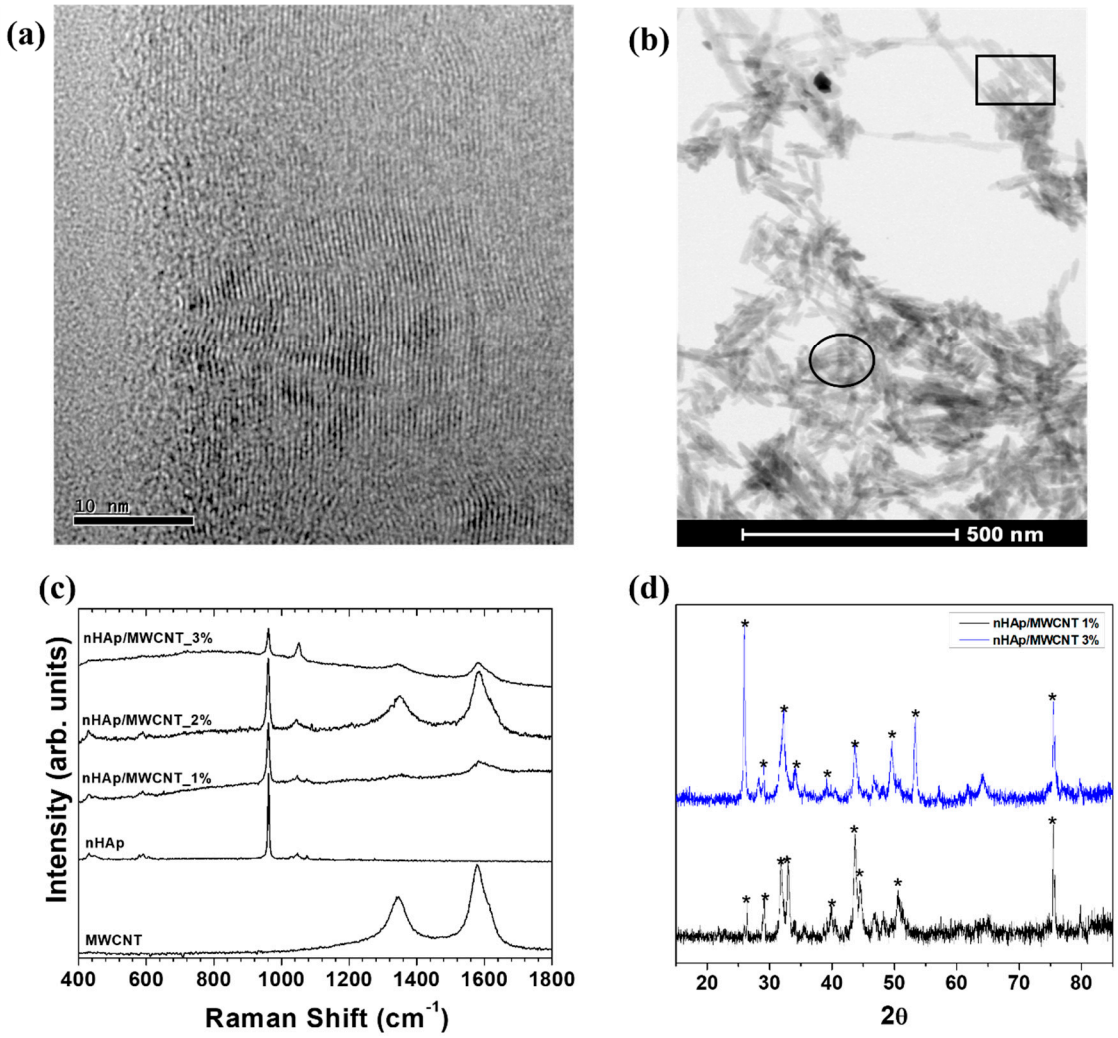

Figure 1. Characterization of MWCNT, nHAp/MWCNT composites and 316L stainless steel alloys covered by nHAp/MWCNT composites. **(a)** HR-TEM illustrates the internal structure of MWCNT showing the walls. **(b)** SEM identified typical needle-like crystals deposited onto MWCNT. Square illustrates the MWCNT covered by nHAp crystals and circle illustrates a region containing pure nHAp crystals. **(c)** Raman spectra collected from 316L stainless steel were consistent with those of nHAp structure, and vibrational modes associated to carbonate and phosphate phase were identified. D and G band from the MWCNT are also identified. **(d)** XRD collected from the top of

Preprints (www.preprints.org) | NOT PEER-REVIEWED | Posted: 24 May 2018 doi:10.20944/preprints201805.0336.v1

Peer-reviewed version available at Materials 2018, 11, 1555; doi:10.3390/ma11091555

electrodeposited nHAp/MWCNT films. Clearly, the nHAp phase was correctly indexed using a JCPDS card: 024-0033 (identified using *).

Fig. 2a1-a3 shows the morphology of nHAp deposited onto 316L stainless steel alloys. Typical plate-like crystals were obtained (**Fig. 2a1**), which is a common morphology addressed to electrodeposited nHAp. A micro-rough film was obtained (Ra=2.63), as shown in **Fig. 2a2**. More details about roughness can be seen from the 3D construction in **Fig. 2a3**. When nHAp/MWCNT composite (1%) was associated with electrolytic solution, needle-like structures were obtained (**Fig 2b1**). This is more common when a rougher surface is used as the working electrode during electrophoretic process (specially TiO_2 nanotubes [19]). **Fig. 2b2** illustrates the roughness of obtained thin films. Clearly, we obtained a rougher structure that was 4-fold lower than those obtained by nHAp without MWCNT. More details can be seen from the 3D construction (**Fig. 2b3**). This difference in structure can be associated to the presence of carbon nanotubes, which act as growth nuclei for the crystals. A similar crystal morphology was identified when 3% of nHAp/MWCNT composite was used (**Fig. 2c1**). The roughness (**Fig. 2c2**, Ra=0.63) and 3D (**Fig. 2c3**) aspects are practically the same as 1%.

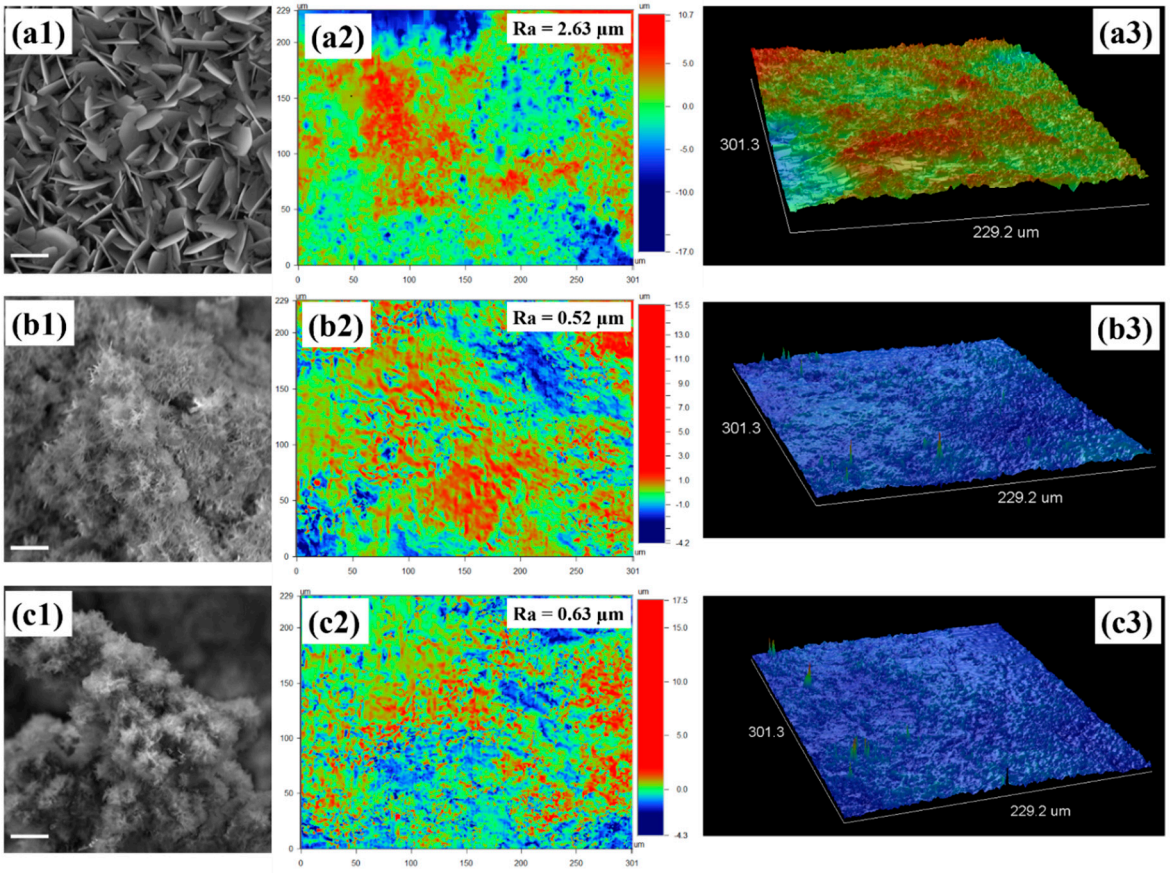

Figure 2. SEM and optical profilometry collected from deposited nHAp and nHAp/MWCNT films on stainless steel alloys. **(a1)** SEM illustrated plate-like crystals of nHAp electrodeposited onto 316L stainless steel alloy. **(a2)** Optical images from profilometry collected at the top of nHAp thin films electrodeposited onto 316L stainless steel. **(e3)** 3D constructions extracted from the top of 316L stainless steel alloy. **(b1)** SEM illustrating needle-like crystals electrodeposited onto 316L stainless steel alloy. **(b2)** Optical images from profilometry collected at the top of nHAp/MWCNT thin films electrodeposited onto 316L stainless steel. **(c3)** 3D constructions collected from the top of 316L stainless steel alloy illustrating nHAp/MWCNT 1% electrodeposited onto 316L stainless steel. **(c1)** SEM illustrated needle-like crystals electrodeposited onto 316L stainless steel alloy. **(c2)** Optical images from profilometry collected at the top of nHAp/MWCNT thin films electrodeposited onto 316L stainless steel. **(c3)** 3D constructions extracted from the top of 316L stainless steel alloy

Preprints (www.preprints.org) | NOT PEER-REVIEWED | Posted: 24 May 2018 doi:10.20944/preprints201805.0336.v1

Peer-reviewed version available at Materials 2018, 11, 1555; doi:10.3390/ma11091555

illustrating nHAp/MWCNT 3% elecrodeposited onto 316L stainless steel. SEM scale bars from Fig.2 a1, b1, and c1 is 2 μm.

To the best of our knowledge, this is the first report that nHAp/MWCNT composites were associated with electrolyte, adjusted to Ca/P=1.67, and a potential was applied to obtain thin films. We also analyzed gene expression related to osteogenic process using these new composites. These findings have important implications for the modification of metal alloys and have great promise for use in biomedical applications. More details about the biological tests are show in **Fig. 3**.

The control group (-, the only group with cells), when compared to the groups of materials (316L, nHAp, nHAp/MWCNT 1% and nHAp/MWCNT 3%), did not present significant statistical difference (<0.01, **Fig. 3a**). Thus, the assay indicates that the materials (316L, nHAp, nHAp/MWCNT 1% and nHAp/MWCNT 3%) did not produce a cytotoxic effect in the MG-63 strain. *In vitro* analysis using osteoblasts indicate that materials containing MWCNTs and nHAp demonstrate high proliferation, cell adhesion and no toxic effects. These results agree with those presented by other authors who used MWCNTs and HAp with polymeric materials [11,20-23]. The HAp, as well as the MWCNTs, when used separately, also did not demonstrate cytotoxicity and had an antibacterial effect, thus suggesting great potential for several biomedical applications [24,25].

The expression of genes involved in bone mineralization and maturation in the osteoblastic cells was analyzed when in contact with the materials (316L, nHAp, nHAp/MWCNT 1% and nHAp/MWCNT 3%) after the 14-day period (**Fig. 3b-3d**). **Fig. 3d** shows a significant increase in the expression of the OPN gene in the cells of the nHAp/MWCNT 1% and nHAp/MWCNT 3% groups (p<0.01), as well as in the cells of the nHAp group (p<0.05) when compared to control.

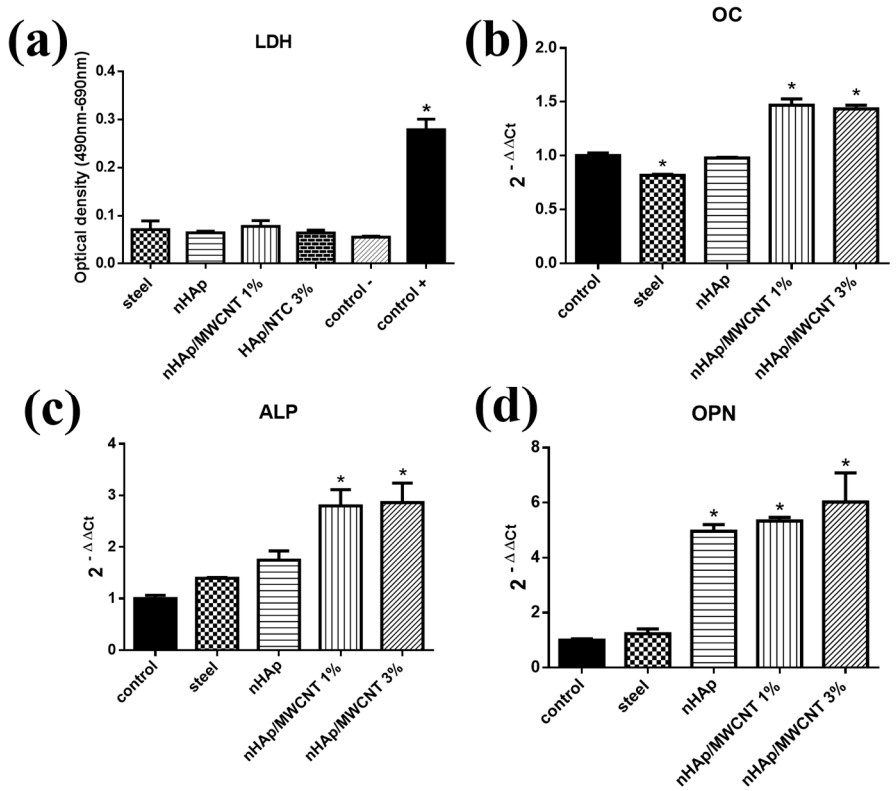

Figure 3. (a) Cell viability assay performed by the LDH assay to analyze different groups (316L stainless steel, nHAp, nHAp/MWCNT 1% and nHAp/MWCNT 3%). The control group (-) represents the negative control for cell death, the control group (+) in which DMSO was added, represents the positive control for cell death. All groups were matched with the control group (-). mRNA genes **(b)** OC, **(c)** ALP and **(d)** OPN expression of MG-63 lineage cells when cultivated with different analyzed groups were similar to the control. The level of expression of each gene was normalized by the expression of -actin. The groups with the samples were compared with the control group (cells

Preprints (www.preprints.org) | NOT PEER-REVIEWED | Posted: 24 May 2018 doi:10.20944/preprints201805.0336.v1

Peer-reviewed version available at Materials 2018, 11, 1555; doi:10.3390/ma11091555

only). Statistical analysis: LDH - Statistical analysis Oneway ANOVA – Kruskal-Wallis test post *p<0.01. Data from each experiment were obtained in triplicate and are presented as mean ± standard deviation. Gene expression - One-way ANOVA – post-test multiple comparisons Dunnett's test *p<0.01; *p<0.05; *p<0.001. (ALP = Alkaline phosphatase, OPN = Osteopontin, OC = Osteocalcin, nHAp = nano-hydroxyapatite, MWCNT = Carbon Nanotubes).

4. Discussion

The osteogenesis process evolves some proteins such as alkaline phosphatase (ALP), osteopontin (OPN), osteocalcin (OC), collagen type I (COL – I) and RUNX – 2 [26,27]. Briefly, ALP occurs in the early stages of osteogenesis and hydrolyzes organic phosphates, causing phosphorus ions to be released, which are important for the process of extracellular matrix mineralization [28]. OPN is secreted in the early stages of osteoblastic development and mineralization, and acts by binding the organic and inorganic phase to promote tissue adhesion. The expression of the OPN gene is also associated with increased cell adhesion [26]. OC is an important factor for bone formation, this gene is expressed only by osteoblasts, and is translated into the most abundant non-collagenous protein found in bone tissue [29].

It is known that important genes related to osteogenesis can be upregulated on rough surfaces and the extracellular matrix, and mineralization *in vitro* was enhanced when cultivated onto rough and porous surfaces. From this, we can infer that the surface morphology is the most important property to control the morphology and promote osteoblast maturation for increased osteogenesis [8,30,31] .

Increased expression of markers such as OPN and OC indicate an advanced differentiation process and determine osteoblastic maturation and bone mineralization. The expression of the OPN gene is also associated with increased cell adhesion. OC is an important factor for bone formation [32]. This gene is expressed only by osteoblasts, and is translated into the most abundant non-collagenous protein found in bone tissue. An important feature of OC is its affinity with Ca^{2+} and hydroxyapatite [29]. The increased expression of the OC observed in nHAp/MWCNT at 1 and 3% (*p<0.01) are most likely associated both to the affinity of nHAp for the synthesized OC and the increased surface roughness (**Fig. 2a-2c**), compared to nHAp alone. The 3D structures highlight (**Fig. 2a-2c**) the surface characterization from the nHAp and nHAp/MWCNT composites.

The OPN expression can be positively correlated to the surface roughness of each of the samples, as previously shown in **Fig. 2a1-c1**. A high expression of the OPN gene occurs in the stage of bone mineralization [33]. Several studies point out that CNTs aid in cell adhesion, which is directly related to the expression of the OPN gene [26,34,35]. The groups containing the HAp/CNT 1%, HAp/CNT 3% samples showed a significant increase in the expression of the alkaline phosphatase (ALP) gene when compared to the control group *p>0.05 (**Fig. 3c**). ALP occurs in the early stages of osteogenesis and plays an important role in bone mineralization. During mineralization, inorganic calcium phosphatase (Ca^{2+}) leads to calcification, with subsequent increase of phosphatase in the site, thus participating in the process of bone formation [35]. Osteoblasts participate in the process of bone formation, synthesizing the organic region of the bone matrix and participating in the mineralization of the matrix due to the presence of calcium phosphate. Osteoblasts, when grown in culture, demonstrate peak alkaline phosphatase activity in the 14-day period [25]. The increase of the ALP gene expression in the groups in contact with the nanocomposites, as observed in this work, indicate the potential ability of this material to increase of the biomineralization of the osteoblasts.

When nHAp/MWCNT composites were used, rougher surfaces were produced, thereby upregulating osteoblast function. This behavior has been widely reported in the literature [36]. However, herein we electrodeposited apatite that has a high bioactivity, facilitating more osteoblast adhesion and maturation. The use of nano-hydroxyapatite on the surface of materials implies an increase in alkaline phosphatase expression [35,37]. Other works have also shown that osteoblasts in contact with composites containing CNT and HAp show an increase in ALP expression after a period of 14 days. The overexpression of this gene is probably associated with an increase in the mineralization and matrix protein deposition [33,37]. Gopi et al had dispersed low amounts of CNT

Preprints (www.preprints.org) | NOT PEER-REVIEWED | Posted: 24 May 2018 doi:10.20944/preprints201805.0336.v1

Peer-reviewed version available at Materials 2018, 11, 1555; doi:10.3390/ma11091555

to apatite electrolyte and performed electrophoresis. The authors obtained a high adherence that was protective against corrosion. However, the authors only evaluated the *in vitro* applications using fibroblast cells [38]. Chakraborty et al. [21] recently electrodeposited phosphate coating with and without CNT. The authors showed that the obtained films were bioactive and were able to improve cell adhesion and growth. However, the authors did not investigate specific osteoblast functions as presented here.

5. Conclusion

A homogeneous and highly crystalline coating onto 316L stainless steel was obtained independent of dispersed nanoparticle. When nHAp/MWCNT composites were used during the electrophoretic process, needle-like crystals were obtained, which produced a rougher coating than those using nHAp alone. All analyzed groups had no cytotoxicity for MG-63 cells. Meanwhile, the presence of nHAp/MWCNT composites upregulated the expression of all analyzed genes related to osteogenesis. Thus, we can conclude that our developed thin films were able to promote the *in vitro* osteoblast maturation and mineralization, a promising first step toward the long-term goal of *in vivo* application to improve bone repair.

Acknowledgements: AOL and FRM would like to thank to National Council for Scientific and Technological Development (CNPq grants numbers AOL 303752/2017-3 and FRM 304133/2017-5) and Universidade Brasil for the scholarships. Special thanks to Jessica Fitzgerald from the Chemical Engineering Writing Center at Northeastern University for English corrections.

References

1. Walczak, J.; Shahgaldi, F.; Heatley, F. In vivo corrosion of 316l stainless-steel hip implants: Morphology and elemental compositions of corrosion products. *Biomaterials* **1998**, *19*, 229-237.
2. Grosgogeat, B.; Reclaru, L.; Lissac, M.; Dalard, F. Measurement and evaluation of galvanic corrosion between titanium/ti6al4v implants and dental alloys by electrochemical techniques and auger spectrometry. *Biomaterials* **1999**, *20*, 933-941.
3. Caicedo, M.S.; Pennekamp, P.H.; McAllister, K.; Jacobs, J.J.; Hallab, N.J. Soluble ions more than particulate cobalt-alloy implant debris induce monocyte costimulatory molecule expression and release of proinflammatory cytokines critical to metal-induced lymphocyte reactivity. *Journal of Biomedical Materials Research Part A* **2010**, *93A*, 1312-1321.
4. JACOBS, J.J.; GILBERT, J.L.; URBAN, R.M. Corrosion of metal orthopaedic implants*. *JBJS* **1998**, *80*, 268-282.
5. González, J.E.G.; Mirza-Rosca, J.C. Study of the corrosion behavior of titanium and some of its alloys for biomedical and dental implant applications. *Journal of Electroanalytical Chemistry* **1999**, *471*, 109-115.
6. Hanawa, T. Metal ion release from metal implants. *Materials Science and Engineering: C* **2004**, *24*, 745-752.
7. Nanci, A.; Wuest, J.D.; Peru, L.; Brunet, P.; Sharma, V.; Zalzal, S.; McKee, M.D. Chemical modification of titanium surfaces for covalent attachment of biological molecules. *Journal of Biomedical Materials Research* **1998**, *40*, 324-335.
8. Groessner-Schreiber, B.; Tuan, R.S. Enhanced extracellular matrix production and mineralization by osteoblasts cultured on titanium surfaces in vitro. *Journal of Cell Science* **1992**, *101*, 209-217.
9. Lobo, A.O.; Marciano, F.R.; Corat, E.J.; Trava-Airoldi, V.J. Processo para produção de nanocompósitos de nanoapatitas e os ditos nanocompósitos. 2013.
10. Rodrigues, B.V.M.; Leite, N.C.; Cavalcanti, B.D.N.; da Silva, N.S.; Marciano, F.R.; Corat, E.J.; Webster, T.J.; Lobo, A.O. Graphene oxide/multi-walled carbon nanotubes as nanofeatured scaffolds for the assisted deposition of nanohydroxyapatite: Characterization and biological evaluation. *International Journal of Nanomedicine* **2016**, *11*, 2569-2585.
11. Lobo, A.O.; Zanin, H.; Siqueira, I.A.W.B.; Leite, N.C.S.; Marciano, F.R.; Corat, E.J. Effect of ultrasound irradiation on the production of nhap/mwcnt nanocomposites. *Materials Science and Engineering: C* **2013**, *33*, 4305-4312.
12. Pfaffl, M.W. A new mathematical model for relative quantification in real-time rt-pcr. *Nucleic acids research* **2001**, *29*.

Preprints (www.preprints.org) | NOT PEER-REVIEWED | Posted: 24 May 2018 doi:10.20944/preprints201805.0336.v1

Peer-reviewed version available at Materials 2018, 11, 1555; doi:10.3390/ma11091555

13. Antunes, E.F.; de Resende, V.G.; Mengui, U.A.; Cunha, J.B.M.; Corat, E.J.; Massi, M. Analyses of residual iron in carbon nanotubes produced by camphor/ferrocene pyrolysis and purified by high temperature annealing. *Applied Surface Science* **2011**, *257*, 8038-8043.
14. Zou, Z.; Lin, K.; Chen, L.; Chang, J. Ultrafast synthesis and characterization of carbonated hydroxyapatite nanopowders via sonochemistry-assisted microwave process. *Ultrasonics Sonochemistry* **2012**, *19*, 1174-1179.
15. Dresselhaus, M.S.; Dresselhaus, G.; Saito, R.; Jorio, A. Raman spectroscopy of carbon nanotubes. *Physics Reports* **2005**, *409*, 47-99.
16. Liao, S.; Xu, G.; Wang, W.; Watari, F.; Cui, F.; Ramakrishna, S.; Chan, C.K. Self-assembly of nano-hydroxyapatite on multi-walled carbon nanotubes. *Acta Biomaterialia* **2007**, *3*, 669-675.
17. Koutsopoulos, S. Synthesis and characterization of hydroxyapatite crystals: A review study on the analytical methods. *Journal of Biomedical Materials Research* **2002**, *62*, 600-612.
18. Gopi, D.; Indira, J.; Prakash, V.C.A.; Kavitha, L. Spectroscopic characterization of porous nanohydroxyapatite synthesized by a novel amino acid soft solution freezing method. *Spectrochimica Acta Part A: Molecular and Biomolecular Spectroscopy* **2009**, *74*, 282-284.
19. Prodana, M.; Duta, M.; Ionita, D.; Bojin, D.; Stan, M.S.; Dinischiotu, A.; Demetrescu, I. A new complex ceramic coating with carbon nanotubes, hydroxyapatite and tio2 nanotubes on ti surface for biomedical applications. *Ceramics International* **2015**, *41*, 6318-6325.
20. Balani, K.; Anderson, R.; Laha, T.; Andara, M.; Tercero, J.; Crumpler, E.; Agarwal, A. Plasma-sprayed carbon nanotube reinforced hydroxyapatite coatings and their interaction with human osteoblasts in vitro. *Biomaterials* **2007**, *28*, 618-624.
21. Chakraborty, R.; Seesala, V.S.; Sen, M.; Sengupta, S.; Dhara, S.; Saha, P.; Das, K.; Das, S. Mwcnt reinforced bone like calcium phosphate—hydroxyapatite composite coating developed through pulsed electrodeposition with varying amount of apatite phase and crystallinity to promote superior osteoconduction, cytocompatibility and corrosion protection performance compared to bare metallic implant surface. *Surface and Coatings Technology* **2017**, *325*, 496-514.
22. Lee, M.; Ku, S.H.; Ryu, J.; Park, C.B. Mussel-inspired functionalization of carbon nanotubes for hydroxyapatite mineralization. *Journal of Materials Chemistry* **2010**, *20*, 8848-8853.
23. Rodrigues, B.V.; Silva, A.S.; Melo, G.F.; Vasconscellos, L.M.; Marciano, F.R.; Lobo, A.O. Influence of low contents of superhydrophilic mwcnt on the properties and cell viability of electrospun poly (butylene adipate-co-terephthalate) fibers. *Materials Science and Engineering: C* **2016**, *59*, 782-791.
24. Shi, C.; Gao, J.; Wang, M.; Fu, J.; Wang, D.; Zhu, Y. Ultra-trace silver-doped hydroxyapatite with non-cytotoxicity and effective antibacterial activity. *Materials Science and Engineering: C* **2015**, *55*, 497-505.
25. Zancanela, D.C.; Sper Simão, A.M.; Matsubara, E.Y.; Rosolen, J.M.; Ciancaglini, P. Defective multilayer carbon nanotubes increase alkaline phosphatase activity and bone-like nodules in osteoblast cultures. *Journal of Nanoscience and Nanotechnology* **2016**, *16*, 1437-1444.
26. Prado, R.F.d.; de Oliveira, F.S.; Nascimento, R.D.; de Vasconcellos, L.M.R.; Carvalho, Y.R.; Cairo, C.A.A. Osteoblast response to porous titanium and biomimetic surface: In vitro analysis. *Materials Science and Engineering: C* **2015**, *52*, 194-203.
27. Becker, J.; Lu, L.; Runge, M.B.; Zeng, H.; Yaszemski, M.J.; Dadsetan, M. Nanocomposite bone scaffolds based on biodegradable polymers and hydroxyapatite. *Journal of Biomedical Materials Research Part A* **2015**, *103*, 2549-2557.
28. Bellows, C.G.; Aubin, J.E.; Heersche, J.N.M. Differential effects of fluoride during initiation and progression of mineralization of osteoid nodules formed in vitro. *Journal of Bone and Mineral Research* **1993**, *8*, 1357-1363.
29. Zhang, S.; Yang, Q.; Zhao, W.; Qiao, B.; Cui, H.; Fan, J.; Li, H.; Tu, X.; Jiang, D. In vitro and in vivo biocompatibility and osteogenesis of graphene-reinforced nanohydroxyapatite polyamide66 ternary biocomposite as orthopedic implant material. *International Journal of Nanomedicine* **2016**, *11*, 3179-3189.
30. Lincks, J.; Boyan, B.D.; Blanchard, C.R.; Lohmann, C.H.; Liu, Y.; Cochran, D.L.; Dean, D.D.; Schwartz, Z. Response of mg63 osteoblast-like cells to titanium and titanium alloy is dependent on surface roughness and composition. *Biomaterials* **1998**, *19*, 2219-2232.
31. Bagherifard, S.; Hickey, D.J.; de Luca, A.C.; Malheiro, V.N.; Markaki, A.E.; Guagliano, M.; Webster, T.J. The influence of nanostructured features on bacterial adhesion and bone cell functions on severely shot peened 316l stainless steel. *Biomaterials* **2015**, *73*, 185-197.

Preprints (www.preprints.org) | NOT PEER-REVIEWED | Posted: 24 May 2018 doi:10.20944/preprints201805.0336.v1

Peer-reviewed version available at Materials 2018, 11, 1555; doi:10.3390/ma11091555

32. Beck, G.R.; Zerler, B.; Moran, E. Phosphate is a specific signal for induction of osteopontin gene expression. *Proceedings of the National Academy of Sciences* **2000**, *97*, 8352-8357.
33. Shao, W.; He, J.; Sang, F.; Ding, B.; Chen, L.; Cui, S.; Li, K.; Han, Q.; Tan, W. Coaxial electrospun aligned tussah silk fibroin nanostructured fiber scaffolds embedded with hydroxyapatite–tussah silk fibroin nanoparticles for bone tissue engineering. *Materials Science and Engineering: C* **2016**, *58*, 342-351.
34. Sawase, T.; Jimbo, R.; Baba, K.; Shibata, Y.; Ikeda, T.; Atsuta, M. Photo-induced hydrophilicity enhances initial cell behavior and early bone apposition. *Clinical Oral Implants Research* **2008**, *19*, 491-496.
35. Vedakumari, W.S.; Priya, V.M.; Sastry, T.P. Deposition of superparamagnetic nanohydroxyapatite on iron–fibrin substrates: Preparation, characterization, cytocompatibility and bioactivity studies. *Colloids and Surfaces B: Biointerfaces* **2014**, *120*, 208-214.
36. Smith, L.L.; Niziolek, P.J.; Haberstroh, K.M.; Nauman, E.A.; Webster, T.J. Decreased fibroblast and increased osteoblast adhesion on nanostructured naoh-etched plga scaffolds. *International Journal of Nanomedicine* **2007**, *2*, 383-388.
37. Thakur, T.; Xavier, J.R.; Cross, L.; Jaiswal, M.K.; Mondragon, E.; Kaunas, R.; Gaharwar, A.K. Photocrosslinkable and elastomeric hydrogels for bone regeneration. *Journal of Biomedical Materials Research Part A* **2016**, *104*, 879-888.
38. Gopi, D.; Shinyjoy, E.; Sekar, M.; Surendiran, M.; Kavitha, L.; Sampath Kumar, T.S. Development of carbon nanotubes reinforced hydroxyapatite composite coatings on titanium by electrodeposition method. *Corrosion Science* **2013**, *73*, 321-330.